Brigita Tomšič, Špela Bajrič, Kaja Cergonja, Gracija Čepič, Ana Gerl, Egshig Ladislav Varga, Marina Panoska, Svjetlana Peulić, Jasna Skoko, Marija Gorjanc, Barbara Simončič
University of Ljubljana, Faculty of Natural Sciences and Engineering, Aškerčeva 12, 1000 Ljubljana, Slovenia

Tailoring of Multifunctional Cotton Fabric by Embedding a TiO_2+ZnO Composite into a Chitosan Matrix

Oblikovanje večfunkcionalne bombažne tkanine z vgraditvijo kompozita TiO_2+ZnO v matrico hitozana

Original scientific article/*Izvirni znanstveni članek*
Received/*Prispelo* 6-2023 • Accepted/*Sprejeto* 6-2023

Prof dr. Barbara Simončič
E-mail: barbara.simoncic@ntf.uni-lj.si
ORCID ID: 0000-0002-6071-8829

Abstract

The use of nanomaterials to functionalise textiles offers new opportunities for chemical modification of textile fibres' surfaces to achieve multifunctional protective properties. In this study, novel coatings were tailored on cotton fabric by embedding a mixture of TiO_2 and ZnO nanoparticles (NPs) of different molar ratios into a chitosan polymer matrix. The excitation energies of the TiO_2+ZnO composites generated in the coatings ranged from 3.20 eV to 3.25 eV, indicating that the photocatalytic performance of the functionalised cotton was driven by UV light. The presence of TiO_2+ZnO composites increased the UV protection factor (UPF) of the cotton fabric from 4.2 for the untreated sample to 15–21 for the functionalised samples. The UPF values of the coatings slightly decreased after repeated washing. The ZnO in the TiO_2+ZnO composites conferred biocidal activity to the coatings, which were resistant to washing at higher ZnO concentrations. In addition, the TiO_2 in the TiO_2+ZnO composites was responsible for the enhanced photocatalytic self-cleaning of the functionalised cotton, which was observed during the initial period of illumination at lower ZnO concentrations in the composite. The main advantage of these TiO_2+ZnO composite coatings is their multifunctionality, which cannot be provided by single-component TiO_2 or ZnO coatings. Moreover, these coatings have wide-ranging practical applications, as they were composed of commercially available nanomaterials and were applied using conventional pad–dry–cure equipment.

Keywords: titanium dioxide, zinc oxide, chitosan, coating, cotton, UV protection, antimicrobial activity, photocatalytic self-cleaning

Izvleček

Uporaba nanomaterialov za funkcionalizacijo tekstilij ponuja nove možnosti kemijske modifikacije površine tekstilnih vlaken za dosego multifunkcionalnih zaščitnih lastnosti. V raziskavi je bila na bombažni tkanini oblikovana nova prevleka z vgraditvijo mešanice nanodelcev (ND) TiO_2 in ZnO različnih molarnih razmerij v matrico hitozana. Energije za vzbujanje oblikovanih kompozitov TiO_2+ZnO v prevleki so bile med 3,20 eV in 3,25 eV, kar pomeni, da je za fotokatalitsko delovanje funkcionaliziranega bombaža potrebna UV-svetloba. Prisotnost kompozita TiO_2+ZnO je povečala UV zaščitni faktor (UZF) s 4,2 za neapretiran bombaž na 15–21 za funkcionalizirane vzorce. Vrednosti UZF-prevlek so se po večkratnem pranju nekoliko zmanjšale. ZnO je kompozitu TiO_2+ZnO zagotovil biocidno aktivnost, ki je bila pri višjih koncentracijah ZnO pri pranju obstojna. TiO_2 je kompozitu TiO_2+ZnO zagotovil izboljšano fotokatalitsko samočistilnost funkcionaliziranega bombaža, ki je bila opazna pri začetnih časih osvetljevanja in pri nižjih koncentracijah ZnO v

kompozitu. Glavna prednost kompozitnih prevlek TiO_2+ZnO je njihova večfunkcionalnost, ki je z enokomponentnimi prevlekami TiO_2 ali ZnO ni bilo mogoče doseči. Prevleke imajo široko praktično uporabo, saj vključujejo komercialno dosegljive nanomateriale in so nanesene s konvencionalno opremo za impregniranje, sušenje in kondenziranje.
Ključne besede: titanov dioksid, cinkov oksid, hitozan, prevleka, bombaž, UV-zaščita, protimikrobna aktivnost, fotokatalitska samočistilnost

1 Introduction

In the last decade, the use of nanomaterials for the functionalisation of textiles has greatly increased, as they have advantages over classical finishing agents, including a high surface-to-volume ratio, which significantly increases their chemical reactivity and functionality, even at low concentrations. As inorganic nanomaterials, TiO_2 and ZnO nanoparticles (NPs) are of great importance due to their exceptional physicochemical and optical properties; they confer multifunctionality to textile fibres, including the functions of photocatalytic self-cleaning, antibacterial activity, UV protection, and thermal stability [1–9]. Both NPs are characterised by thermal, chemical, and photochemical stability, non-toxicity, biocompatibility, and a low price.

As metal oxides, TiO_2 and ZnO are semiconductor materials with photocatalytic activity under UV irradiation [10–12]. The absorption of UV radiation is related to the UV protection properties of TiO_2 and ZnO. At the same time, the excitation of semiconductors enables the formation of reactive oxygen species (ROS) on the surface of semiconductors; these are very important for the degradation of various organic compounds and the antimicrobial activity of TiO_2 and ZnO. All of these functional properties are directly affected by the particle size, morphology, and concentration. In addition, the photocatalytic efficiency of semiconductors could be significantly enhanced and moved into the visible range through various surface and interface engineering strategies, including coupling with other semiconductors to create semiconductor–semiconductor heterojunctions [13, 14]. This offers the possibility for the chemical modification of textile fibres with a composite TiO_2 and ZnO heterojunction, which would improve the photocatalytic performance of the coating.

The major drawback in tailoring textiles' functionalities by using inorganic NPs is their low affinity to textile fibres. Therefore, in order to increase the adsorption capacity of NPs and enhance their adhesive force, various approaches have been pursued, such as anchoring NPs to textile fibres with crosslinking agents or incorporating NPs into the polymer matrix formed on the fibre surface [15–19]. As a nanocomposite matrix, chitosan has already attracted attention due to its exceptional properties, such as its natural origin, non-toxicity, biocompatibility, biodegradability, and low cost [20]. Several amino and hydroxyl groups in the chitosan polymer structure are capable of creating electrostatic attractive and hydrogen bonds that enable the embedding of various NPs into the polymer matrix [21–32]. The ability of chitosan to embed semiconductor metal oxides can make it an effective platform for photocatalytic performance [21, 28, 32, 33]. Moreover, since chitosan is known as an absorbent that can absorb different organic substances by attracting –OH and $–NH_2$ functional groups, this could greatly improve the adsorption–photocatalysis process [32, 34–36].

Considering all of these aspects, the aim of this research was to develop a novel multifunctional coating on cellulose fibres by embedding a TiO_2+ZnO composite into a chitosan matrix and applying it to a cotton substrate with the facile pad–dry–cure process. Recently, the quaternary ammonium chitosan Schiff base was already synthesised and used for the in-situ synthesis of TiO_2 and ZnO NPs from the corresponding precursors with the ultrasonic irradiation process [37], which limited this research to the laboratory level. Our idea was to extend this research by using commercial products and conventional application equipment, thus providing the possibility for the functionalisation of textiles at the industrial level, which is of great practical significance. To investigate the influence of the ratio of concentrations between TiO_2 and ZnO in the composite on the functional properties, the concentration of TiO_2 was kept constant while the concentration of ZnO was varied. To determine the possibility of the formation of a TiO_2+ZnO heterojunction in the coating, the optical properties of the composites were investigated. In addition, special attention was paid to the UV protection, antibacterial activity, and photocatalytic self-cleaning of the coatings.

2 Experimental

2.1 Materials

Woven fabric made of 100% cotton in plain weave with a mass per unit area of 119 g/m^2 was kindly provided by Tekstina d.o.o. (Ajdovščina, Slovenia). The fabric was pre-scoured, bleached, and mercerized. Commercially available TiO_2 anatase nanopowder with a particle size of less than 25 nm and ZnO nanopowder with 30 nm particles were purchased from Sigma Aldrich. Chitosan solution with a viscosity of 159 mPa and a deacetylation degree of 95% was purchased from Chitoclear (Primex, Iceland).

2.2 Functionalisation of the cotton fabric

The chitosan solution was prepared at a concentration of 0.2% in deionized water in the presence of 1.0% acetic acid. The solution was left for 24 hours with constant stirring. Then, the TiO_2 and ZnO NPs were dispersed in the chitosan solution in the appropriate ratios by sonicating them for 30 minutes with a UP 200St ultrasonicator (Hielscher, Germany). For this purpose, the concentration of the TiO_2 NPs remained constant at 1.0%, while the concentration of the ZnO NPs varied between 0.5% and 2.0%. For comparison, a single component of TiO_2 at 1.0% and 3% and a single component of ZnO at 3% were dispersed in the chitosan solution, and a mixture of 1.0% TiO_2 and 2.0% ZnO was dispersed in deionized water without chitosan.

The prepared dispersions were applied to cotton fabric by using the pad–dry–cure method. The coating procedure involved the complete immersion of the cotton samples in the appropriate dispersions at room temperature, followed by squeezing on a two-roll padder (Mathis, Switzerland) for a wet pickup of 85% ± 5%, drying at 100 °C for 3 minutes, and curing at 150 °C for 2 minutes. The samples were then rinsed with distilled water to remove the unbound coatings. After rinsing, the functionalised cotton samples were air-dried. The sample codes corresponding to the applied coatings are listed in Table 1.

2.3 Washing procedure

The functionalised cotton samples were washed five times in a Gyrowash (James Heal, UK). The washing bath consisted of 2 g/L of nonionic detergent at a goods-to-liquor ratio of 1 : 20. Each washing cycle was performed at 40 °C for 30 minutes. After each washing cycle, the samples were rinsed twice with the same amount of distilled water as for the washing process and left to dry.

2.4 Analyses and measurements

2.4.1 Scanning electron microscopy (SEM) and energy-dispersive X-ray spectroscopy (EDS)

The morphological characteristics of the studied cotton samples were examined with a JSM 6060 LV scanning electron microscope (JEOL, Japan). Prior to the examination, the samples were coated with a thin layer of gold to ensure conductivity. The samples were scanned at a magnification of 2000x.

EDS analysis was performed by using a field-emission scanning electron microscope (FEG-SEM Thermo Scientific Quattro S ThermoFischer Scientific, USA). Sample analysis was performed by using an Oxford Instruments Ultim Max 65 energy-dispersive detector (EDS) and the AZtec software. The samples were coated with a thin carbon layer prior to the analysis to provide conductivity and, thus, improve the quality of the images.

2.4.2 Fourier transform infrared (FT-IR) spectroscopy

Chemical changes in the cotton samples after functionalisation were observed by using an FT-IR

Table 1: Sample codes according to the coatings

Sample code	Functionalisation procedure
CO_UN	Untreated cotton sample
CO/Ch+Ti1	Cotton sample functionalised with a mixture of 0.2% chitosan and 1% TiO_2
CO/Ch+Ti1+Zn0.5	Cotton sample functionalised with a mixture of 0.2% chitosan, 1% TiO_2, and 0.5% ZnO
CO/Ch+Ti1+Zn1	Cotton sample functionalised with a mixture of 0.2% chitosan, 1% TiO_2, and 1.0% ZnO
CO/Ch+Ti1+Zn1.5	Cotton sample functionalised with a mixture of 0.2% chitosan, 1% TiO_2, and 1.5% ZnO
CO/Ch+Ti1+Zn2	Cotton sample functionalised with a mixture of 0.2% chitosan, 1% TiO_2, and 2.0% ZnO
CO/Ch+Ti3	Cotton sample functionalised with a mixture of 0.2% chitosan and 3% TiO_2
CO/Ch+Zn3	Cotton sample functionalised with a mixture of 0.2% chitosan and 3% ZnO

Spectrum 3 spectrometer (Perkin Elmer, UK). Spectra were recorded between 4000 cm^{-1} and 600 cm^{-1} with a resolution of 4 cm^{-1} and an average of 120 spectra per sample.

2.4.3 UV–Vis spectroscopy and determination of the optical band-gap energy (E_g)

The transmission spectra of the untreated and functionalised cotton samples were recorded by using a Lamda 850+ UV/Vis spectrophotometer (Perkin Elmer, United Kingdom) that was equipped with a reflection module—a 150 mm integration sphere—and fully controlled by a computer running the WinLab 6 UV software. Transmittance (T) was measured in the wavelength range of 200–800 nm. Three measurements were made for each sample at different angles of warp alignment, and the average value of T at each wavelength was calculated. The transmission spectra were converted into absorption spectra by using the following equation:

$$A = -\log T \tag{1}$$

where A is the absorbance.

From the absorption spectra, the E_g values of the TiO_2, ZnO, and TiO_2+ZnO coatings on the cotton samples were determined by using the Tauc relation, in which the energy-dependent absorption coefficient, α, is related to the incident photon energy, $h{\cdot}\nu$ (Reddy 2002, Karkare 2015). This relationship is expressed by the following equation [38]:

$$(\alpha h\nu)^n = K\left(h\nu - E_g\right) \tag{2}$$

where K is the absorption constant, h is the Planck constant, ν is the frequency of light, and n is an index characterizing the optical absorption process. The latter is equal to two for the direct band-gap transitions proposed for TiO_2 and ZnO [38]. According to the Tauc method, the value of E_g was graphically determined from the Tauc plot as the value of the photon energy obtained when the linear part of the plot was extrapolated to $\alpha = 0$.

2.4.4 UV protection properties

The UV protection properties of the untreated and functionalised cotton samples were determined according the EN 13758-1: 2001 standard by measuring the UV transmission spectra (Section 2.4.3). The main values of T were calculated at wavelengths of 315–400 nm (UVA), 290–315 nm (UVB), and 290–400 nm (UVR). The ultraviolet protection factor (UPF) was calculated as follows:

$$\mathrm{UPF} = \frac{\sum_{290}^{400} E(\lambda)\cdot\varepsilon(\lambda)\cdot\Delta\lambda}{\sum_{290}^{400} E(\lambda)\cdot\varepsilon(\lambda)\cdot T(\lambda)\cdot\Delta\lambda} \tag{3}$$

where $E(\lambda)$ is the solar spectral irradiance, $\varepsilon(\lambda)$ is the relative erythemal effectiveness, $\Delta(\lambda)$ is the wavelength interval, and $T(\lambda)$ is the spectral transmittance at the wavelength λ. The UPF rating and protection categories were determined from the UPF values, which were calculated according to the Australian/New Zealand Standard for Sun-Protective Clothing—Evaluation and Classification (AS/NZS 4399, 2020), where UPF values of 15– correspond to the "minimum protection" category, UPF values of 30– correspond to the "good protection" category, and UPF values of 50– correspond to the "excellent protection" category.

In addition, the reflection (R) of the samples in the wavelength range of 250–450 nm was also recorded.

2.4.5 Antibacterial activity

The antibacterial activity of the untreated and functionalised cotton samples against the Gram-positive bacteria *Staphylococcus aureus* (*S. Aureus*; ATCC 6538) and the Gram-negative bacteria *Escherichia coli* (*E. Coli*; ATCC 25922) was evaluated by using the AATCC 100-2012 method. First, the samples were cut into a circular shape of 4.8 ± 0.1 cm in diameter. Then, a sufficient number of samples were used for the complete uptake of 1 mL of inoculum. After 24 hours of incubation at 37 °C, the samples were washed with neutralizing solution and vigorously shaken for one minute. Serial dilutions of the liquid were then prepared and spread on nutrient agar. After incubation, the number of bacterial colonies per sample was determined. The bacterial reduction (R) was calculated by using the following equation:

$$\mathrm{R} = \frac{(\mathrm{B\text{-}C})}{\mathrm{B}} \times 100 \tag{4}$$

where B is the number of bacterial colony-forming units (CFU) recovered from the inoculated untreated control samples in the jar at an incubation time of 24 hours, and C is the number of bacteria recovered from the inoculated functionalised test samples in the jar at an incubation time of 24 hours.

2.4.6 Photocatalytic self-cleaning activity

The photocatalytic self-cleaning activity of the untreated and the functionalised samples was determined based on the photodegradation of a Rhodamine B (RhB) dye under simulated sunlight. For this purpose, the samples were immersed in the RhB solution for 30 seconds and then air-dried and illuminated for five hours at 35 °C and 70% humidity in a Xenon Alpha device (Atlas, USA) equipped with a visible xenon arc lamp (radiation attitude: 0.8–2.5 kVA; extended radiation range: 300–400 nm). Before and after each hour of illumination, the colour coordinates L^*, a^*, b^*, and Y in the CIELAB colour space were determined for the studied samples by using a Datacolor Spectro 1050 spectrophotometer (Datacolor, USA). Measurements were performed with a 9 mm aperture under D65 illumination and an observation angle of 10°. Ten measurements were performed for each sample, and the colour difference (ΔE^*_{ab}) was calculated by using the following equation [39]:

$$\Delta E^*_{ab} = \sqrt{(\Delta L^*)^2 + (\Delta a^*)^2 + (\Delta b^*)^2} \quad (5)$$

where ΔL^*, Δa^*, and Δb^* are the differences in the lightness, green–red, and blue–yellow colour coordinates, respectively, calculated between the illuminated and non-illuminated samples. Colour fading in the samples due to the photodegradation of the RhB dye was also estimated from the Y coordinate, which was the luminance and represented the perceived brightness. The efficiency of colour fading was calculated as the ratio of Y_t/Y_0, where Y_0 and Y_t represent the Y coordinates before and after a certain irradiation time, respectively.

3 Results and discussion

3.1 Morphological and chemical properties

The morphological properties of the untreated and functionalised cotton samples are shown in Figure 1. In the SEM images, it is evident that compared to the untreated cotton sample, the application of TiO_2 and ZnO NPs increased the roughness of the fibres, as there were visible agglomerates of both TiO_2 and ZnO NPs on the fibre surface. It is also evident that the number of NPs on the fibre surface increased when the concentration of ZnO NPs in the dispersion was increased from 0.5% to 2%. The comparison of the CO/Ch+Ti3 and CO/Ch+Zn3 samples showed that at the same concentration of 3.0% in the dispersion, the loading of ZnO NPs was higher than that of TiO_2 NPs, with agglomerates of a smaller size being uniformly distributed in the chitosan matrix on the surface of the cotton fibres. The presence of TiO_2 and ZnO NPs on the surface of the cotton fibres was confirmed by the EDS analysis (Figure 2), as characteristic peaks were observed at 0.5, 4.5, and 4.9 keV for TiO_2 and at 1.0, 8.6, and 9.4 keV for ZnO in the CO/Ch+Ti1+Zn2 sample.

The chemical characteristics of the untreated and functionalised cotton samples were investigated by using FT-IR analysis, and the results are shown in Figure 3. The ATR spectra of all samples, regardless of the chemical modification, exhibited the bands characteristic of the fingerprint of cellulose fibres and adsorbed water [40, 41]. Thus, the band at 2890 cm^{-1} was attributed to the valence vibration of the CH_2 and CH_3 groups, the band at 1640 cm^{-1} corresponded to the deformation vibration of the

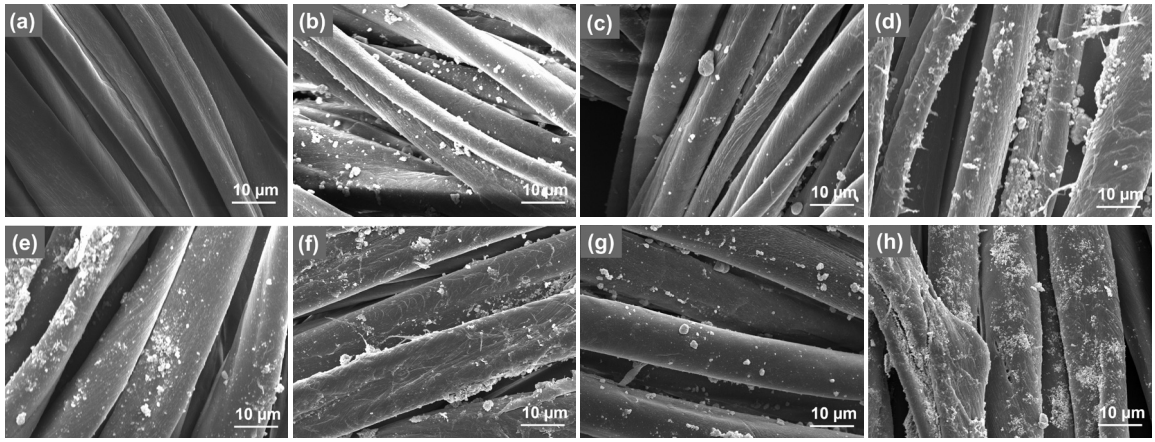

Figure 1: SEM images of the untreated (a) and functionalised cotton samples: CO/Ch+Ti1 (b), CO/Ch+Ti1+Zn0.5 (c), CO/Ch/Ti1+Zn1 (d), CO/Ch+Ti1+Zn1.5 (e), CO/Ch/Ti1+Zn2 (f), CO/Ch+Ti3 (g), and CO/Ch/Zn3 (h)

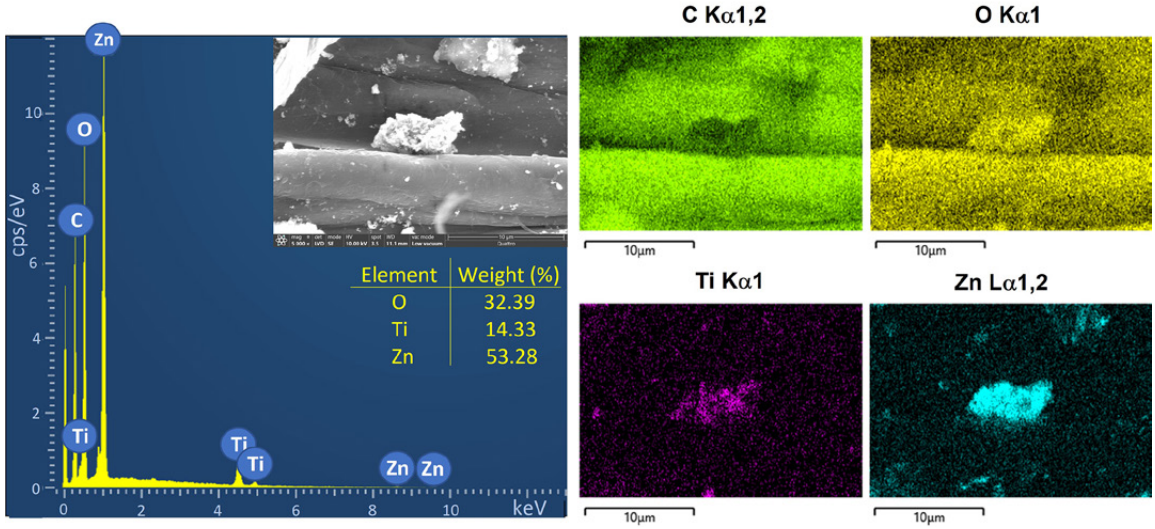

a) b)

Figure 2: EDS spectrum (a) and element mapping images of C, O, Zn, and Ti (b) in the CO/Ch/Ti1+Zn2 sample

OHO groups, the band at 1160 cm^{-1} corresponded to the asymmetric valence vibration of the C-C groups, the band at 1100 cm^{-1} was attributed to the asymmetric valence vibration of the C-O-C groups, the band at 1052 cm^{-1} was attributed to the asymmetric stretching of the glycosidic ring, the bands at 1025 cm^{-1} and 997 cm^{-1} were attributed to the valence vibration of the C-OH groups of the secondary and primary alcohols, respectively, and the band at 900 cm^{-1} corresponded to the asymmetric valence vibration of the C_1-O-C_4 groups. For the functionalised CO/Ch+Ti3, CO/Ch+Zn3, and CO/Ch+Ti1+Zn1 samples, no characteristic bands of TiO_2 and ZnO were detected, indicating the absence of chemical interactions of these NPs with the functional groups of cotton cellulose [41]. For these samples, the typical band of N-H bending of the amino groups of chitosan at 1580 cm^{-1} could not be detected, as the concentration of chitosan was too low (0.2%). Moreover, the band at 1601 cm^{-1}, which was characteristic of the C=O group of the amide group, was blurred by the vibrations of the cellulose macromolecules [40].

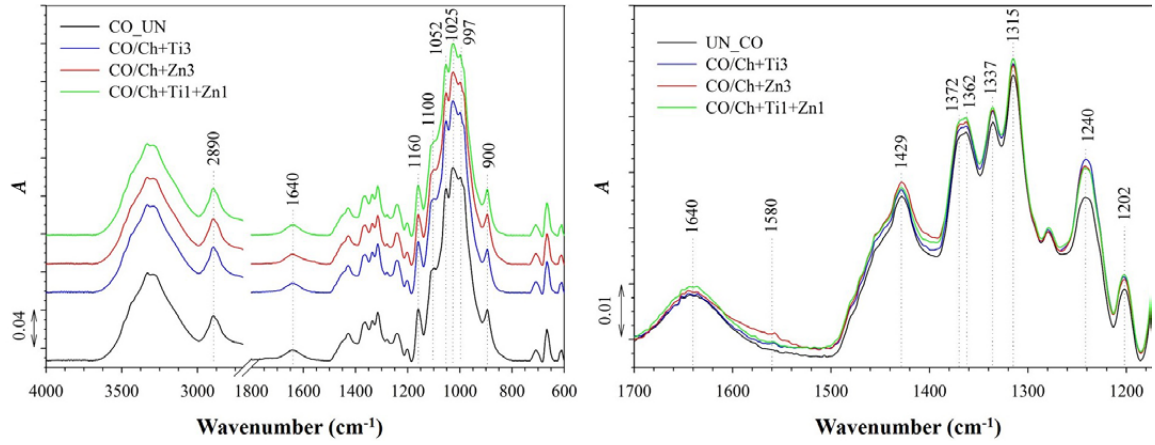

a) b)

Figure 3: IR ATR spectra of the untreated cotton sample (CO_UN) and the chemically modified CO/Ch+Ti1+Zn1, CO/Ch+Ti3, and CO/Ch+Zn3 samples in the spectral region of 4000–600 cm^{-1} (a) and in the spectral region of 1700–1180 cm^{-1} (b)

3.2 Optical properties

The influence of the presence of the coatings on the optical properties of the functionalised cotton samples is shown in Figure 4. From the absorption spectra (Figure 4a and 4b), it can be seen that the absorption of UV radiation was significantly increased for all of the functionalised samples compared to the untreated cotton sample, which was attributed to the presence of TiO_2 and ZnO NPs, which are known to be effective UV absorbers. A comparison of the CO/Ch+Ti1 and CO/Ch+Ti3 samples (Figure 4a) shows that increasing the TiO_2 concentration from 1% to 3% in the dispersion did not significantly change the absorbance of the functionalised cotton samples. Moreover, a comparison of the CO/Ch+Ti3 and CO/Ch+Zn3 samples with the same 3% NPs in the dispersions reveals that the absorption efficiency of TiO_2 in the UVA region from 320 to 400 nm was significantly lower than that of ZnO. For the cotton samples with TiO_2+ZnO composites (Figure 4b), the absorption in the entire UV region was lower than that of the samples with single-component TiO_2 or ZnO coatings. It is also evident that increasing the concentration of ZnO NPs in the TiO_2+ZnO composite beneficially affected the absorption efficiency of the samples in the UVA region.

The Tauc plots (Figure 4c) and the calculated values of E_g (Figure 4d) show that the excitation energies of TiO_2 and ZnO were 3.25 eV and 3.20 eV, respectively, and that the energies required for the excitation of the TiO_2+ZnO composites were between 3.20 eV and 3.25 eV. All of these estimated excitation energies were those of UV rays, and there was not a bathochromic shift in the absorption of the TiO_2+ZnO composites to visible light. This clearly indicated that the simple mixing of TiO_2 and ZnO NPs in the dispersion was not sufficient to form a heterojunction with visible-light-driven photocatalytic performance.

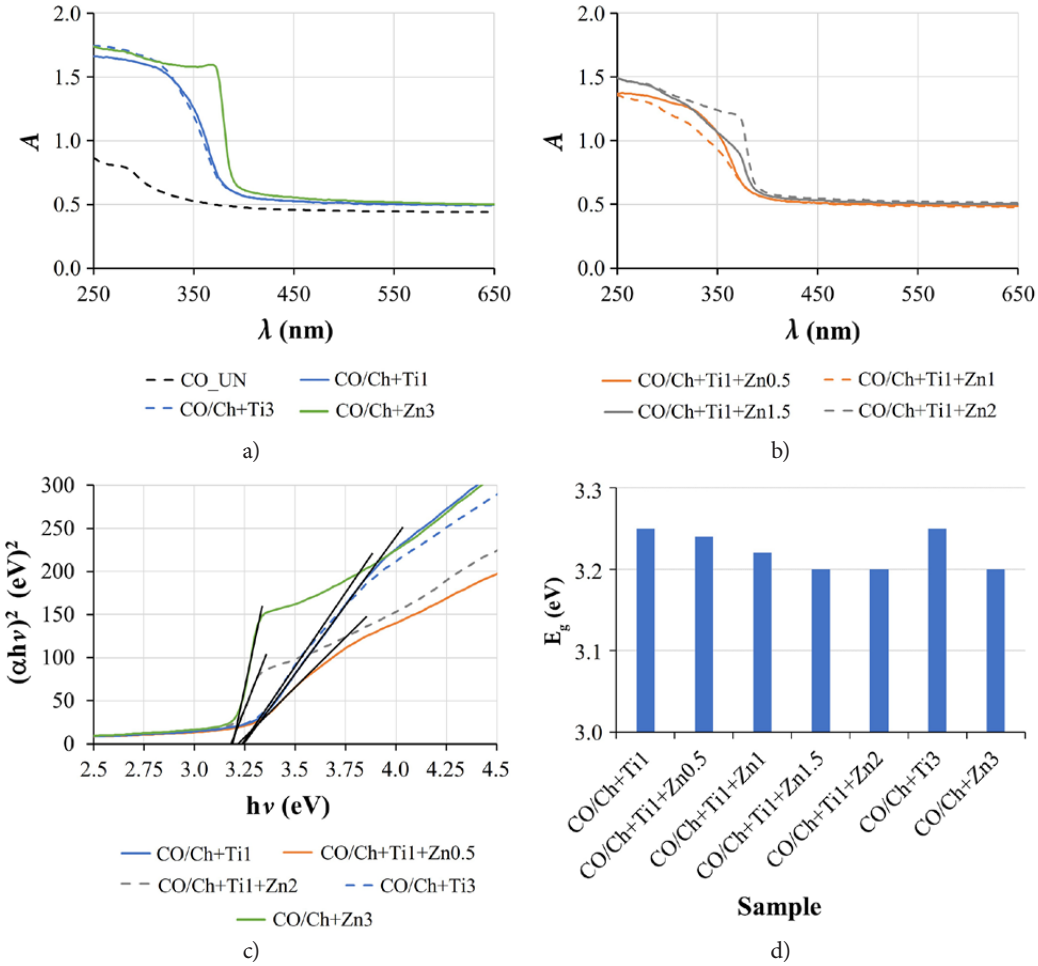

Figure 4: Absorption spectra of the untreated and functionalised cotton samples (a, b); Tauc plots of the representative samples (c) and E_g values of the functionalised cotton sample

3.3 UV protection properties

Since the UV protection properties were directly related to the transmission of UV rays through the cotton fabric, the transmission and reflection spectra of the untreated and the functionalised cotton samples were recorded, and the results are presented in Figure 5 and Table 2. The results clearly show that the presence of all coatings significantly reduced the transmittance and the reflectance of the cotton fabric. Since the transmittance of the CO/Ch+Ti3 and CO/Ch+Zn3 samples was very similar in the UVB region (280–320 nm), the transmittance in the UVA region of the CO/Ch+Zn3 sample was much lower than that of the CO/Ch+Ti3 sample, which was beneficial for UV protection. In addition, the CO/Ch+Ti3 sample also exhibited lower transmission of UV rays than that of all cotton samples with the TiO_2+ZnO composites. Since the lower transmission of UV rays through the functionalised cotton sample was accompanied by lower UV light reflection, this indicated that the UV-blocking mechanism of TiO_2 and ZnO was based on the absorption of UV rays. These results are in good agreement with the absorption spectra (Figures 4a and 4b).

The lower the transmittance of the cotton fabric for UV rays, the higher the UPF value. The results in Table 2 show that the UPF value of the untreated cotton sample was very low, indicating insufficient protection against UV radiation. The CO/Ch+Ti1, CO/Ch+Ti3, and CO/Ch+Zn3 samples provided good protection against UV radiation, with UPF values of 32.3, 32.4, and 39.2, respectively. Since the transmission of UV rays through the samples with the coatings of the two-component TiO_2 and ZnO NPs was generally high compared to that of the cotton samples with the single-component TiO_2 or ZnO coatings, their UPF values were lower—as expected—and were in the range of 15–25, which is described as providing minimum protection. After five repetitions of washing, the UPF values of all functionalised samples decreased, indicating that the functionalisation of the cotton fibres was not permanent, that the chitosan matrix did not chemically bind the TiO_2 and ZnO NPs to the cotton fibres, and that they gradually released from the samples during the washings. These results are consistent with the results of the FT-IR analysis.

3.4 Antibacterial activity

The reduction in bacterial growth in the functionalised cotton samples compared to the untreated cotton sample is shown in Figure 6. It was found that even at the highest concentration of 3% in the dispersion, TiO_2 could not provide a sufficient reduction in both the Gram-positive bacteria *S. aureus* and the Gram-negative bacteria *E. coli*. Accordingly, the CO/Ch+Ti1 and CO/Ch+Ti3 samples did not exhibit antibacterial properties. In contrast, the addition of ZnO to the TiO_2 and ZnO mixture dramatically increased the antibacterial activity of the functionalised cotton samples and reduced the growth of both bacteria by 100%, even at the lowest concentration of 0.5% ZnO. Increasing the ZnO concentration from 1.0% to 2.0% had a beneficial effect on the durability of the antibacterial properties of the samples, resulting in a 100% bacterial reduction after five repeated washings for the CO/Ch+Ti1+Zn1, CO/Ch+Ti1+Zn1.5, and CO/Ch+Ti1+Zn2 samples. Similar results were also obtained for the CO/Ch+Zn3 sample. Although these

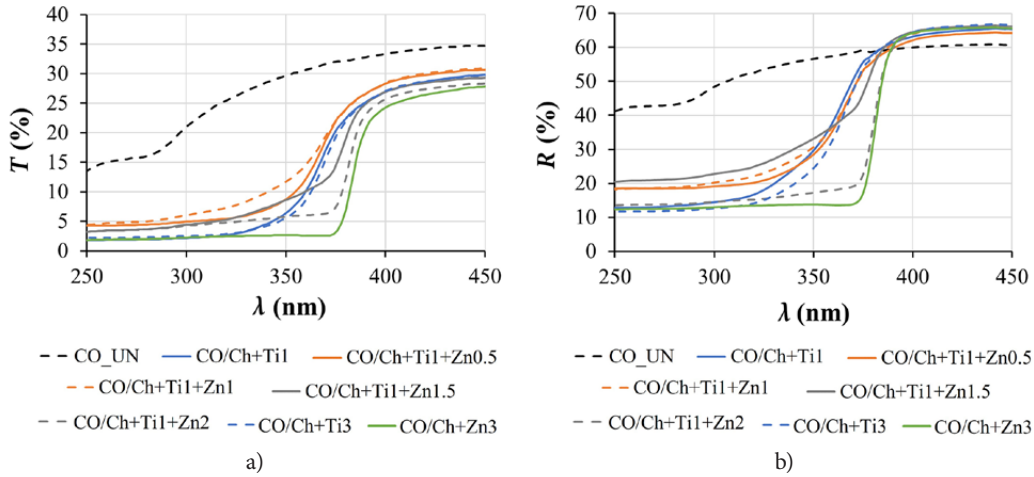

a) b)

Figure 5: Transmittance (a) and reflectance (b) versus wavelength for the untreated and chemically modified samples

Table 2: The arithmetic mean of T in the UVA, UVB, *and* UVR *ranges and the* UVR *protection categories for the untreated and functionalised cotton samples according to the Australian/New Zealand Standard Sun-Protective Clothing—Evaluation and Classification—before and after five repetitions of washing*

Sample	Number of washings	*T* (UVA) (%)	*T* (UVB) (%)	*T* (UVR) (%)	UPF	UVR protection category [a)]
CO_UN	0	30.0	21.3	28.0	4.2	NR
	5	28.2	18.6	24.8	5.8	NR
CO/Ch+Ti1	0	12.5	2.21	10.1	32.3	G
	5	19.9	4.9	16.1	15.4	M
CO/Ch+Ti1+Zn0.5	0	14.6	5.0	12.4	17.1	M
	5	17.8	4.7	14.7	11.7	NR
CO/Ch+Ti1+Zn1	0	16.11	6.14	13.8	15.6	M
	5	21.8	10.3	19.1	8.4	NR
CO/Ch+Ti1+Zn1.5	0	12.7	4.5	10.8	18.7	M
	5	22.1	10.5	19.5	8.2	NR
CO/Ch+Ti1+Zn2	0	9.8	4.3	8.5	20.8	M
	5	18.5	8.2	16.1	10.5	NR
CO/Ch+Ti3	0	12.0	2.5	9.8	32.4	G
	5	16.8	3.8	13.8	19.9	M
CO/Ch+Zn3	0	6.7	2.3	5.7	39.2	G
	5	11.9	5.8	10.5	15.5	M

[a)] NR – non rateable, M – minimum protection, G – good protection, E – excellent protection

results could not be directly compared with those obtained by Rafaee et al. [37], who synthesised two TiO_2/ZnO nanocomposites with different molar ratios of TiO_2:ZnO, a similar trend could be found, as the ZnO-rich TiO_2/ZnO nanocomposite provided better antibacterial activity than that of the TiO_2-rich one. However, in that study, no single-component nanocomposites were used as references.

3.5 Photocatalytic self-cleaning

The photocatalytic self-cleaning properties of the functionalised samples were determined based on the photodegradation of RhB dye in the functionalised samples in comparison with the untreated cotton sample after different illumination times (Figure 7). The results show that increasing the illumination time caused the photodegradation of

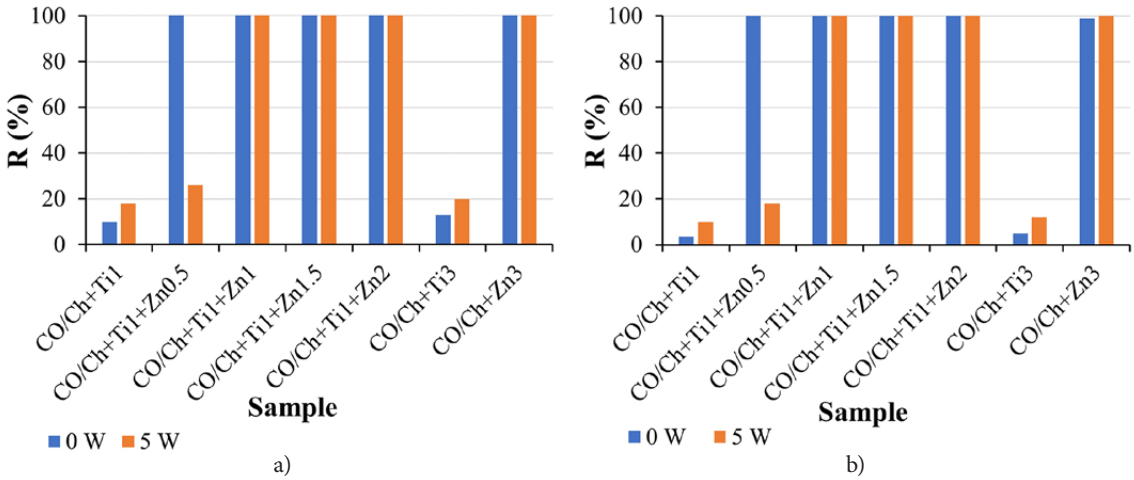

Figure 6: Bacterial reduction, R, *of the functionalised cotton samples against S. aureus (a) and E. coli (b) before (0 W) and after five (5 W) washings*

the RhB dye in all samples, including the untreated one, resulting in an increase in the ΔE^*_{ab} value (Figure 7a), as well as a fading of the colour (Figure 7b). It can also be seen that the CO/Ch+Ti1 and CO/Ch+Ti3 samples exhibited the highest photocatalytic self-cleaning efficiency, resulting in a drastic colour change in the RhB dye after the first hour of illumination. The higher the TiO_2 concentration, the greater the colour change. The results also showed that the degradation of the RhB dye in the CO/Ch+Ti1 and CO/Ch+Ti3 samples was completed after 3 hours of illumination, which meant that the colour could not fade further with a longer illumination time. Figure 7a also reveals that ZnO alone in the CO/Ch+Zn3 sample did not show any photocatalytic performance. This was likely the reason for why the presence of ZnO in the mixture with TiO_2 hindered the photocatalytic self-cleaning of the coatings in comparison with the single-component TiO_2 coatings. While photocatalytic self-cleaning properties were observed for the CO/Ch+Ti1+Zn0.5 and CO/Ch+Ti1+Zn1 samples in the initial phase of illumination, this phenomenon was less pronounced for the coatings containing ZnO in higher concentrations (the CO/Ch+Ti1+Zn1.5 and CO/Ch+Ti1+Zn2 samples).

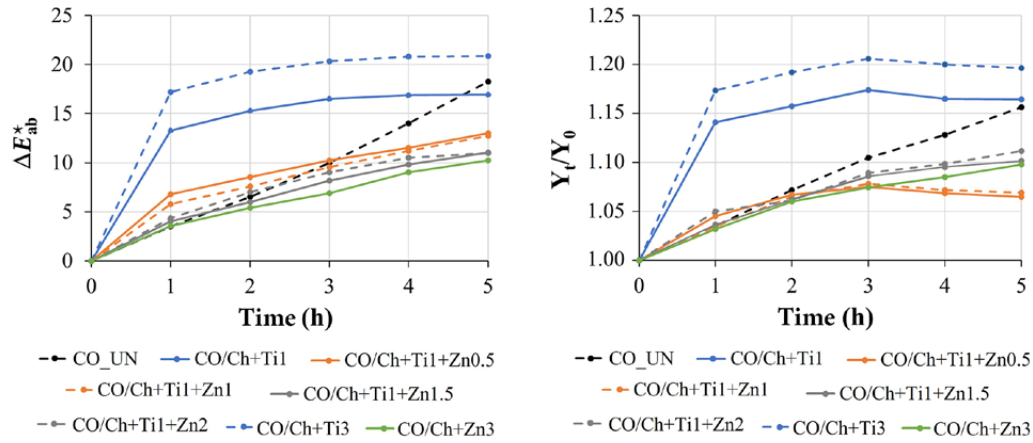

Figure 7: The colour difference (Δ), (a), and Y coordinate ratio (b) between the samples stained with the RhB dye and illuminated for different periods of time and the stained unilluminated samples

In contrast to all functionalised samples, the colour change in the untreated cotton sample gradually increased during the illumination period, resulting in an increase in the ΔE^*_{ab} value, which even exceeded the ΔE^*_{ab} value determined for the CO/Ch+Ti1 sample. However, a look at the digital images of the samples in Figure 8 reveals that after five hours of illumination, the untreated cotton sample (CO_UN) stained with the RhB dye was more intensely coloured than the CO/Ch+Ti1 and CO/Ch+Ti3 samples, as well as the CO/Ch+Ti1+Zn1 and CO/Ch+Ti1+Zn2 samples. To find the reason for these ΔE^*_{ab} and Y values in Figures 7a and 7b, the colour coordinates CIE a^* and CIE b^* of the dyed samples were examined (Figure 9). The results show that both colour coordinates (CIE a* and CIE b*) of the functionalised samples were significantly different from those of the untreated sample even before illumination and that after illumination, the differences in the CIE a^* and CIE b^* values were significantly smaller than those of the untreated sample. This phenomenon was particularly evident for the CIE b^* coordinate, which represents the yellow–blue axis. While the CIE b^* value of the untreated sample changed from more to less blue during the illumination, the CIE b^* coordinates of the CO/Ch+Ti1 and CO/Ch+Ti3 samples were negative and very close to zero, and they hardly changed with the illumination time. This indicated that the colour was more greyish, which was also consistent with the Y coordinate, which actually decreased after three hours of illumination. This clearly affected the value of ΔE^*_{ab}. Figure 8 also shows that the affinity of the RhB dye for the CO/Ch+Ti1 and CO/Ch+Ti3 samples was significantly higher than for the untreated cotton sample and the samples with coatings that included ZnO, resulting in a higher colour yield. However, the colour of these samples faded almost completely after only one hour of illumination.

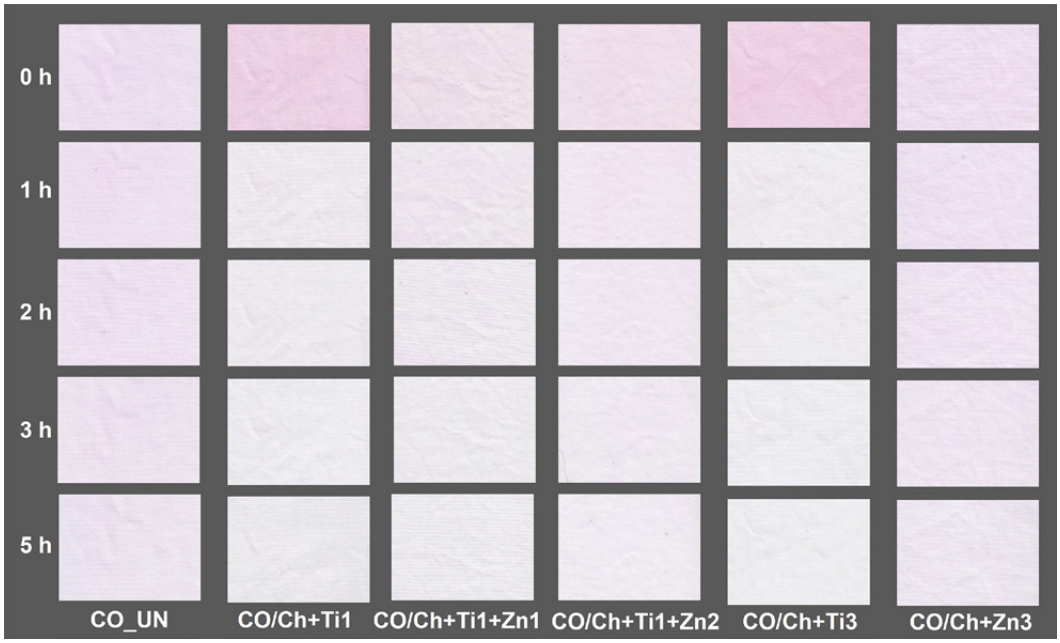

Figure 8: Digital images of the samples stained with RhB dye before and after different illumination times

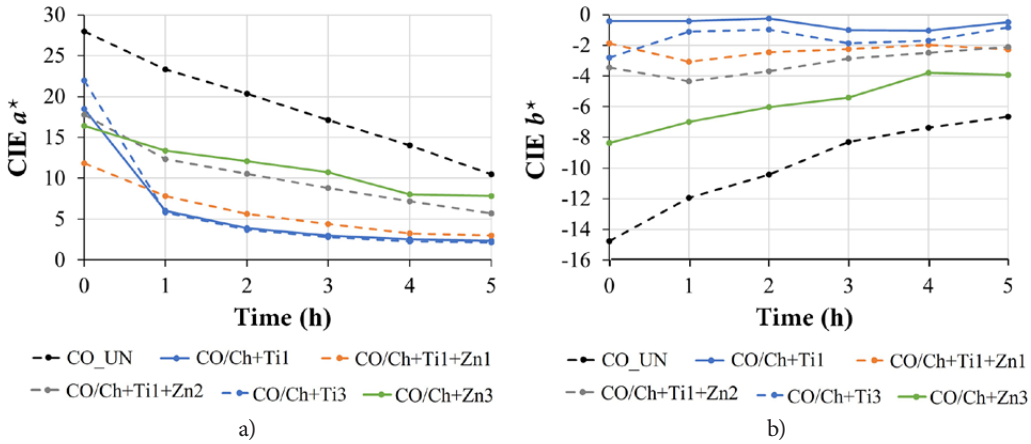

Figure 9: CIE a (a) and CIE b* (b) of the samples stained with RhB dye before and after different illumination times*

4 Conclusion

In summary, a novel and facile method was developed for the preparation of a multifunctional coating on a cotton fabric consisting of a TiO_2+ZnO composite embedded in a chitosan matrix. Although the simple mixing of commercial TiO_2 and ZnO NPs in a dispersion was not sufficient to form a heterojunction with enhanced photocatalytic performance, the presence of both TiO_2 and ZnO in the coating conferred multifunctional properties to the cotton fibres that could not be achieved with single-component TiO_2/chitosan and ZnO/chitosan coatings. Namely, the coatings simultaneously exhibited the following functionalities:

- Minimum UV protection properties that were less effective than those of the single-component TiO_2/chitosan and ZnO/chitosan coatings.
- Bactericidal activity due to the presence of ZnO, which could not be achieved even at the highest TiO_2 concentration in the single-component TiO_2/chitosan coatings.
- The improved photocatalytic self-cleaning, which was not as effective as that in the single-component TiO2/chitosan coating but was much more effective than that in the single-component ZnO/chitosan coating.

The use of commercially available TiO_2 and ZnO NPs, chitosan, and the pad–dry–cure application

process with conventional equipment enables the functionalisation of textiles on an industrial scale, which is of great practical significance.

Acknowledgment

This research was carried out within the framework of the courses on Advanced Finishing Processes and Chemical Functionalisation of Textiles in the Master Study Programme for Textile and Clothing Planning. The research was co-funded by the Slovenian Research Agency (Program P2-0213, Infrastructural Centre RIC UL-NTF).

References

1. RADETIĆ, M. Functionalization of textile materials with TiO_2 nanoparticles. *Journal of Photochemistry and Photobiology C: Photochemistry Reviews*, 2013, **16**, 62–76, doi: 10.1016/j.jphotochemrev.2013.04.002.
2. RIVERO, P.J., URRUTIA, A., GOICOECHEA, J., ARREGUI, F.J. Nanomaterials for functional textiles and fibers. *Nanoscale Research Letters*, 2015, **10**, 1–22, doi: 10.1186/s11671-015-1195-6.
3. VERBIČ, A., GORJANC, M., SIMONČIČ, B. Zinc oxide for functional textile coatings: recent advances. *Coatings*, 2019, **9**(9), 1–26, doi: 10.3390/coatings9090550.
4. ANAYA-ESPARZA, L.M., RUVALCABA-GÓMEZ, J.M., MAYTORENA-VERDUGO, C.I., GONZÁLEZ-SILVA, N., ROMERO-TOLEDO, R., AGUILERA-AGUIRRE, S., PÉREZ-LARIOS, A., MONTALVO-GONZÁLEZ, E. Chitosan-TiO_2: a versatile hybrid composite. *Materials*, 2020, **13**(4), 1–27, doi: 10.3390/ma13040811.
5. GRANADOS, A., PLEIXATS, R., VALLRIBERA, A. Recent advances on antimicrobial and anti-inflammatory cotton fabrics containing nanostructures. *Molecules*, 2021, **26**(10), 1–22, doi: 10.3390/molecules26103008.
6. RASHID, M.M., SIMONČIČ, B., TOMŠIČ, B. Recent advances in TiO_2-functionalized textile surfaces. *Surfaces and Interfaces*, 2021, **22**, 1–33, doi: 10.1016/j.surfin.2020.100890.
7. BANDARA, T.M.W.J., HANSADI, J.M.C., BELLA, F. A review of textile dye-sensitized solar cells for wearable electronics. *Ionics*, 2022, **28**, 2563–2583, doi: 10.1007/s11581-022-04582-8.
8. ABOU ELMAATY, T.M., ELSISI, H., ELSAYAD, G., ELHADAD, H., PLUTINO, M.R. Recent advances in functionalization of cotton fabrics with nanotechnology. *Polymers*, 2022, **14**(20), 1–17, doi: 10.3390/polym14204273.
9. DEJENE, B.K., GELETAW, T.M. A review of plant-mediated synthesis of zinc oxide nanoparticles for self-cleaning textiles. *Research Journal of Textile and Apparel*, 2023, ahead-of-print, doi: 10.1108/RJTA-12-2022-0154.
10. LIU, G., YANG, H.G., PAN, J., YANG, Y.Q., LU, G.Q.M., CHENG, H.M. Titanium dioxide crystals with tailored facets. *Chemical Reviews*, 2014, **114**(19), 9559–9612, doi: 10.1021/cr400621z.
11. PARIHAR, V., RAJA, M., PAULOSE, R. A brief review of structural, electrical and electrochemical properties of zinc oxide nanoparticles. *Reviews on Advanced Materials Science*, 2018, **53**, 119–130, doi: 10.1515/rams-2018-0009.
12. NAM, Y., LIM, J.H., KO, K.C., LEE, J.Y. Photocatalytic activity of TiO_2 nanoparticles: a theoretical aspect. *Journal of Materials Chemistry A*, 2019, **7**(23), 13833–13859, doi: 10.1039/c9ta03385h.
13. SHEN, R., JIANG, C., XIANG, Q., XIE, J., LI, X. Surface and interface engineering of hierarchical photocatalysts. *Applied Surface Science*, 2019, **471**, 43–87, doi: 10.1016/j.apsusc.2018.11.205.
14. SINGH, J., KUMAR, S., RISHIKESH, MANNA, A.K., SONI, R.K. Fabrication of ZnO–TiO_2 nanohybrids for rapid sunlight driven photodegradation of textile dyes and antibiotic residue molecules. *Optical Materials*, 2020, **107**, 1–12, doi: 10.1016/j.optmat.2020.110138.
15. LIU, S., ZHANG, Q., XU, Z., YANG, S., LIU, H. Surface modification of TiO_2/SiO_2 composite hydrosol stabilized with polycarboxylic acid on Kroy-process wool fabric. *Journal of Adhesion Science and Technology*, 2017, **31**(11), 1209–1228, doi: 10.1080/01694243.2016.1249687.
16. MARKOVIĆ, D., DEEKS, C., NUNNEY, T., RADOVANOVIĆ, Ž., RADOIČIĆ, M., ŠAPONJIĆ, Z., RADETIĆ, M. Antibacterial activity of Cu-based nanoparticles synthesized on the cotton fabrics modified with polycarboxylic acids. *Carbohydrate Polymers*, 2018, **200**, 173–182, doi: 10.1016/j.carbpol.2018.08.001.
17. SARWAR, N., ASHRAF, M., MOHSIN, M., REHMAN, A., YOUNUS, A., JAVID, A., IQBAL, K., RIAZ, S. Multifunctional formaldehyde free finishing of cotton by using metal oxide nanoparticles and ecofriendly cross-linkers. *Fibers and Polymers*, 2019, **20**, 2326–2333, doi: 10.1007/s12221-019-9170-y.

18. IVANUŠA, M., KUMER, B., PETROVČIČ, E., ŠTULAR, D., ZORC, M., JERMAN, I., GORJANC, M., TOMŠIČ, B., SIMONČIČ, B. Eco-friendly approach to produce durable multifunctional cotton fibres using TiO_2, ZnO and Ag NPs. *Nanomaterials*, 2022, **12**(18), 1–21, doi: 10.3390/nano12183140.
19. RASHID, M.M., TOMŠIČ, B., SIMONČIČ, B., JERMAN, I., ŠTULAR, D., ZORC, M. Sustainable and cost-effective functionalization of textile surfaces with Ag-doped TiO_2/polysiloxane hybrid nanocomposite for UV protection, antibacterial and self-cleaning properties. *Applies Surface Science*, 2022, **595**, 1–15, doi: 10.1016/j.apsusc.2022.153521.
20. SILVA, A.O., CUNHA, R.S., HOTZA, D., MACHADO, R.A.F. Chitosan as a matrix of nanocomposites: a review on nanostructures, processes, properties, and applications. *Carbohydrate Polymers*, 2021, **272**, 1–13, doi: 10.1016/j.carbpol.2021.118472.
21. IBRAHIM, N.A., EID, B.M., EL-AZIZ, E.A., ELMAATY, T.M.A., RAMADAN, S.M. Loading of chitosan – nano metal oxide hybrids onto cotton/polyester fabrics to impart permanent and effective multifunctions. *International Journal of Biological Macromolecules*, 2017, **105**(1), 769–776, doi: 10.1016/j.ijbiomac.2017.07.099.
22. HOLDER, S.L., LEE, C.H., POPURI, S.R. Simultaneous wastewater treatment and bioelectricity production in microbial fuel cells using cross-linked chitosan-graphene oxide mixed-matrix membranes. *Environmental Science and Pollution Research,* 2017, **24**, 13782–13796, doi: 10.1007/s11356-017-8839-2.
23. MISHRA, S.K., TEOTIA, A.K., KUMAR, A., KANNAN, S. Mechanically tuned nanocomposite coating on titanium metal with integrated properties of biofilm inhibition, cell proliferation, and sustained drug delivery. *Nanomedicine: Nanotechnology, Biology, and Medicine (Nanomedicine: NBM)*, 2017, **13**(1), 23–35, doi: 10.1016/j.nano.2016.08.010.
24. NIVETHAA, E.A.K., DHANAVEL, S., NARAYANAN, V., STEPHEN, A. Chitosan stabilized Ag-Au nanoalloy for colorimetric sensing and 5-fluorouracil delivery. *International Journal of Biological Macromolecules*, 2017, **95**, 862–872, doi: 10.1016/j.ijbiomac.2016.10.066.
25. KIM, J.S., LIM, J.K., PARK, J.S. Enhancement of mechanical stability and ionic conductivity of chitosan-based solid polymer electrolytes using silver nanowires as fillers. *Bulletin of the Korean Chemical Society*, 2019, **40**(9), 898–905, doi: 10.1002/bkcs.11844.
26. ABED, A., BOUAZIZI, N., GIRAUD, S., EL ACHARI, A., CAMPAGNE, C., THOUMIRE, O., EL MOZNINE, R., CHERKAOUI, O., VIEILLARD, J., AZZOUZ, A. Preparation of a novel composite based polyester nonwovens with high mechanical resistance and wash fastness properties. *Colloids and Surfaces A: Physicochemical and Engineering Aspects*, 2019, **577**, 604–612, doi: 10.1016/j.colsurfa.2019.05.090.
27. WU, C., ZHU, Y., WU, T., WANG, L., YUAN, Y., CHEN, J., HU, Y., PANG, J. Enhanced functional properties of biopolymer film incorporated with curcurmin-loaded mesoporous silica nanoparticles for food packaging. *Food Chemistry*, 2019, **288**, 139–145, doi: 10.1016/j.foodchem.2019.03.010.
28. AZIZ, S.B., KARIM, W.O., GHAREEB, H.O. The deficiency of chitosan: $AgNO_3$ polymer electrolyte incorporated with titanium dioxide filler for device fabrication and membrane separation technology. *Journal of Materials Research and Technology*, 2020, **9**(3), 4692–4705, doi: 10.1016/j.jmrt.2020.02.097.
29. RODRIGUES, C., DE MELLO, J.M.M., DALCANTON, F., MACUVELE, D.L.P., PADOIN, N., FIORI, M.A., SOARES, C., RIELLA, H.G. Mechanical, thermal and antimicrobial properties of chitosan-based-nanocomposite with potential applications for food packaging. *Journal of Polymers and the Environment*, 2020, **28**, 1216–1236, doi: 10.1007/s10924-020-01678-y.
30. HUANG, C., PENG, B. Photocatalytic degradation of patulin in apple juice based on nitrogen-doped chitosan-TiO_2 nanocomposite prepared by a new approach. *LWT – Food Science and Technology*, 2021, **140**, 1–8, doi: 10.1016/j.lwt.2020.110726.
31. ZHANG, X., ZHANG, Z., WU, W., YANG, J., YANG, Q. Preparation and characterization of chitosan/nano-ZnO composite film with antimicrobial activity. *Bioprocess and Biosystems Engineering*, 2021, **44**, 1193–1199, doi: 10.1007/s00449-021-02521-x.
32. XU, Q., WANG, P., ZHANG, Y., LI, C. Durable antibacterial and UV protective properties of cotton fabric coated with carboxymethyl chitosan and Ag/TiO_2 composite nanoparticles. *Fibers and Polymers*, 2022, **23**, 386–395, doi: 10.1007/s12221-021-0352-z.
33. MIDYA, L., SARKAR, A.N., DAS, R., MAITY, A., PAL, S. Crosslinked chitosan embedded TiO_2 NPs and carbon dots-based nanocomposite:

an excellent photocatalyst under sunlight irradiation. *International Journal of Biological Macromolecules*, 2020, **164**, 3676–3686, doi: 10.1016/j.ijbiomac.2020.08.230.

34. CHEN, A.H., LIU, S.C., CHEN, C.Y., CHEN, C.Y. Comparative adsorption of Cu(II), Zn(II), and Pb(II) ions in aqueous solution on the crosslinked chitosan with epichlorohydrin. *Journal of Hazardous Materials*, 2008, **154**(1–3), 184–191, doi: 10.1016/j.jhazmat.2007.10.009.
35. ZAINAL, Z., HUI, L.K., HUSSEIN, M.Z., ABDULLAH, H.A., HAMADNEH, I.K.R. Characterization of TiO2–Chitosan/Glass photocatalyst for the removal of a monoazo dye via photodegradation–adsorption process. *Journal of Hazardous Materials*, 2009, **164**(1), 138–145, doi: 10.1016/j.jhazmat.2008.07.154.
36. ABARNA, B., PREETHI, T., RAJARAJESWARI, G.R. Single-pot solid-state synthesis of ZnO/chitosan composite for photocatalytic and antitumour applications. *Journal of Materials Science: Materials in Electronics*, 2019, **30**, 21355–21368, doi: 10.1007/s10854-019-02512-5.
37. REFAEE, A.A., EL-NAGGAR, M.E., MOSTAFA, T.B., ELSHAARAWY, R.F.M., NASR, A.M. Nano-bio finishing of cotton fabric with quaternized chitosan Schiff base-TiO_2-ZnO nanocomposites for antimicrobial and UV protection applications. *European Polymer Journal*, 2022, **166**, 1–11, doi: 10.1016/j.eurpolymj.2022.111040.
38. KARKARE, M.M. The direct transition and not indirect transition, is more favourable for band gap calculation of anatase TiO_2 nanoparticles. *International Journal of Scientific & Engineering Research*, 2015, **6**(12), 48–53.
39. BERGER-SCHUNN, A. *Practical color measurement*. New York : John Wiley Sons, 1994, p. 39.
40. KRUER-ZERHUSEN, N., CANTERO-TUBILLA, B., WILSON, D.B. Characterization of cellulose crystallinity after enzymatic treatment using Fourier transform infrared spectroscopy (FTIR). *Cellulose*, 2018, **25**, 37–48, doi: 10.1007/s10570-017-1542-0.
41. SOCRATES, G. *Infrared and raman characteristic group frequencies: tables and charts*. 3rd ed. New York : John Wiley & Sons, 2004.